



HAL
open science

Using in situ measurements to experimentally characterize TiO₂ nanoparticle synthesis in a turbulent isopropyl alcohol flame

Benedetta Franzelli, Philippe Scouflaire, Nasser Darabiha

► To cite this version:

Benedetta Franzelli, Philippe Scouflaire, Nasser Darabiha. Using in situ measurements to experimentally characterize TiO₂ nanoparticle synthesis in a turbulent isopropyl alcohol flame. 10th European Combustion Meeting (2021), Apr 2021, Napoli (Virtual conference), Italy. hal-03442004

HAL Id: hal-03442004

<https://hal.science/hal-03442004v1>

Submitted on 22 Nov 2021

HAL is a multi-disciplinary open access archive for the deposit and dissemination of scientific research documents, whether they are published or not. The documents may come from teaching and research institutions in France or abroad, or from public or private research centers.

L'archive ouverte pluridisciplinaire **HAL**, est destinée au dépôt et à la diffusion de documents scientifiques de niveau recherche, publiés ou non, émanant des établissements d'enseignement et de recherche français ou étrangers, des laboratoires publics ou privés.

Using in situ measurements to experimentally characterize TiO₂ nanoparticle synthesis in a turbulent isopropyl alcohol flame

B. Franzelli^{a,*}, P. Scouflaire^a, N. Darabiha^a

^aLaboratoire EM2C, Université Paris-Saclay, CNRS, CentraleSupélec,
1-3 rue du Joliot Curie, 91960 Gif-sur-Yvette, France

Abstract

The objective of the present work is to contribute in understanding TiO₂ nanoparticles production in turbulent spray flames. Multiple in situ diagnostics from combustion research are employed to study the main processes that characterize the spray flame synthesis. In this way, the liquid break-up, the reactive flow and the TiO₂ particles production are analyzed using shadowgraphy, light scattering, global flame luminosity and OH* chemiluminescence techniques.

Measurements showed that it is possible to simultaneously localize by shadowgraphy the spray, the nanoparticles and the hot/cold layer of the flow. Light scattering measurements allow to characterize the TiO₂ nanoparticles distribution in the flame central plane. Spontaneous global emission and OH* chemiluminescence results show quite different reactive flow patterns for liquid with and without TTIP. When TTIP injection is considered, the liquid is localized in a small region close to the injector nozzle where it is dispersed by the oxygen flow resulting in droplets. The liquid droplets rapidly evaporate and TTIP is quasi-immediately converted to TiO₂ nanoparticles. Results show high interactions between nanoparticles and the turbulent eddies. These results illustrate the high potential of in situ optical diagnostics from combustion research to improve the knowledge on flame synthesis of nanoparticles.

1. Introduction

The understanding of the effect of turbulence on nanoparticle synthesis is of great relevance for the combustion community. On the one side, flame synthesis is a promising technique to produce nanoparticles with well-defined characteristics in terms of particles size, morphology and properties. On the other side, what is learnt on the particle dynamics effects in these systems can be applied, to a certain extent, to soot production in turbulent flames.

Laboratory-scale spray flame reactors were developed to improve our understanding on nanoparticles production [1–9]. In specific, ex situ measurements are classically performed to characterize the effect on the total production and the particle properties of the operating conditions, such as temperature, pressure, precursors concentrations. More recently, numerical simulations of flame synthesis have been performed [10–13] to provide a complementary understanding of the different processes occurring in flame synthesis. Unfortunately, their use is quite limited since the modeling of the different physical processes is extremely challenging and additional in situ measurements are needed to characterize the boundary conditions and to validate the simulations.

In this framework, the present study aims to contribute to our understanding of nanoparticles synthesis in turbulent spray flames by investigating a laboratory-scale spray flame reactor using in situ measurements from combustion research. The burner consists of a spray nozzle (where a liquid fuel is atomized via an annular dispersion gas), a pilot premixed ethylene/air flame and an air coflow. The considered liquid fuel is a solution of isopropyl and tetraisopropoxide (TTIP) precursor.

Three main processes characterize the flame: a) the break-up of the liquid injection, b) the reactive flow and c) the production of the particles. The spatial localization

of these three processes is here provided using in situ experimental measurements, classically used in combustion research: a) shadowgraphy and light scattering for the liquid phase, b) flame luminosity and OH* chemiluminescence to characterize the combustion process, c) light scattering to localize TiO₂ nanoparticles.

The paper is organized as follows. First, the experimental setup is described by presenting the flame synthesis burner and the different optical diagnostics considered in this work. Then, the potentials and the difficulties in applying shadowgraphy and light scattering to the characterization of nanoparticle flame synthesis are discussed. Finally, results are presented by looking at the three different processes that characterize nanoparticles flame synthesis.

2. Experimental setup

2.1. Flame synthesis burner

The burner studied in the present work is the same as used in [2–5, 12], the ParteQ GMBH model LS-FSR. The burner, schematically presented in Fig. 1b, allows the stabilisation of a turbulent spray flame, whose luminosity is visualized in Fig. 1a. For this, a mixture of liquid isopropyl alcohol (Sigma Aldrich) and tetraisopropoxide (TTIP) (Sigma Aldrich) with a purity of 97% is injected through a syringe in the center (1 ml of TTIP for 200 ml of isopropyl alcohol). The liquid flow is provided by a Tuthill pump upstream of a mini-Coriolis flowmeter from Bronkhorst. The imposed flow rate is 0.003 NI/min. The liquid jet is surrounded and dispersed by a circular jet of pure oxygen with a flowrate of 5 NI/min. A premixed ethylene-air pilot flame with an equivalence ratio of $\Phi = 1.5$ (oxygen flowrate of 2.5 NI/min and ethylene flowrate of 1.25 NI/min) is needed for the stabilization of the non-premixed flame. The coflow consists of pure nitrogen with a flowrate of 3 NI/min.

*Corresponding author: benedetta.franzelli@centralesupelec.fr

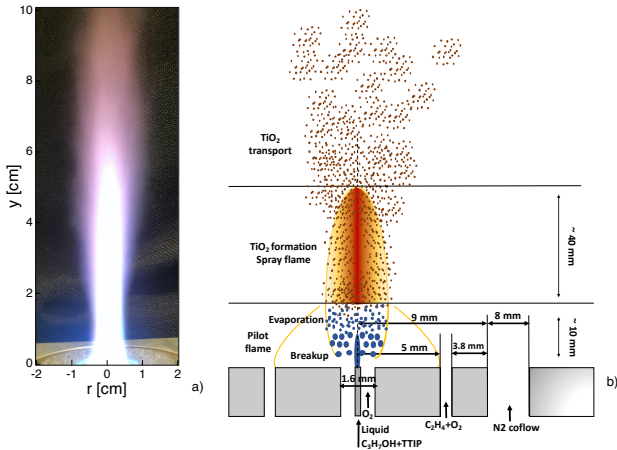


Figure 1: a) Flame luminosity. b) Sketch of the reactor inlet and of the processes inside the reactor.

2.2. In situ optical diagnostics from combustion research

2.2.1. Shadowgraphy

The shadowgraph measurements are performed with a red backlighting system featuring a red LED spot. A schematic presentation of the diagnostic setup is presented in Fig. 2. The red LED spot consists in a 7 cm x 9 cm rectangle of LEDs emitting at a dominant wavelength of 633nm. A frosted glass is placed between the spot and the flame to get a light as homogeneous in space as possible. The spot is fed by a direct current power supply in order to avoid main current frequency interference. A Photron Fastcam SAX2 camera operating at 10000 fps is placed at the opposite side of the LED spot to obtain shadowgraphy images of the flame. It is equipped with a Nikon 105mm f/2.8 lens and a 20 mm extension ring. A filter is placed in front of the camera objective to remove all wavelengths other than 633 nm. Images of 1024x1024 pixels are obtained with a resolution of 40 $\mu\text{m}/\text{px}$. The acquisition gate width is 10 μs .

2.2.2. Global and OH* spontaneous emissions

The same camera used for shadowgraphy at the same position (Fig. 2) is used for measurements of spontaneous global and OH* emissions by turning off the red light source. For global spontaneous emission, no filter is used on the camera and the exposure time is adjusted so as not to saturate the gray levels (25 μs). Regarding the OH* emission, an Asahi 310 nm filter (96SA02), FWHM 10.00 nm is used in front of the camera lens. The exposure time is 100 μs .

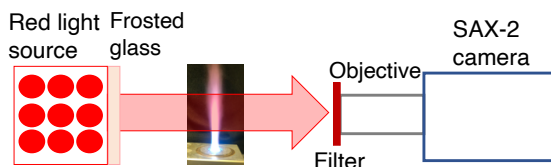


Figure 2: Schematic presentation of the shadowgraphy system.

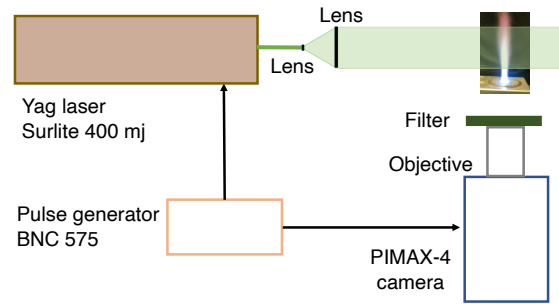


Figure 3: Schematic presentation of the light scattering system.

2.2.3. Light scattering

The light scattering measurement setup is presented in Fig. 3. It comprises a YAG Surlite 400 mJ Continuum laser at 532 nm wavelength is used for the light scattering on the solid particles. A set of two lenses creates a laser sheet of 70 mm high and about 300 μm thickness. The scattering is observed through a Roper PIMAX4 camera (1024 * 1024 pixels) equipped with a Sodem UV lens 100F/2.8 and a 20 mm extension ring. It has a spatial resolution of 60 $\mu\text{m}/\text{px}$. A Semrock FF01 530 FWHM 11 nm filter allows the observation of only light scattering. Both the camera and the laser are synchronized via a pulse generator BNC575. The image acquisition is taken with an gate width of 15 ns and no delay.

3. Using shadowgraphy and light scattering diagnostics to characterize flame synthesis

Multiple quantities can be visualized using the shadowgraphy measurements as illustrated in Figs. 4a-d. First of all, when considering the non-reacting cold case (Fig. 4a), the presence of the liquid jet and of the spray can be detected since the objects between the light source and the camera appear the darker the more they absorb the light. Similarly, the liquid presence is detected in the reacting cases (without and with TTIP injection in Figs. 4b and c, respectively). It can be observed that the liquid phase occupies a smaller region due to its quick evaporation due to the high temperature of the flame.

In the case of TTIP injection (Fig. 4c), spots of light due to diffraction of partially transparent TiO₂ nanoparticles can be observed. Then, it is possible to discriminate spray from TiO₂ nanoparticles by considering dark or bright information. In addition, by post-processing the shadowgraphy image to highlight the gradient regions, as done in Fig. 4d, it is possible to identify the variation of flow density between the ambient fresh air and the high temperature flame burnt gases due to the dependence of the light refractive index on the fluid density. Therefore, thanks to the shadowgraphy, it is possible to get simultaneous information on the localization of spray, of TiO₂ nanoparticles and of the hot/cold gas layer.

Since the shadowgraphy measurements provide line-of-sight-integrated information, light scattering measurements were also performed to investigate spray and TiO₂ nanoparticles distribution at the central plane. An instantaneous result is visualized in Fig. 4e. With this tech-

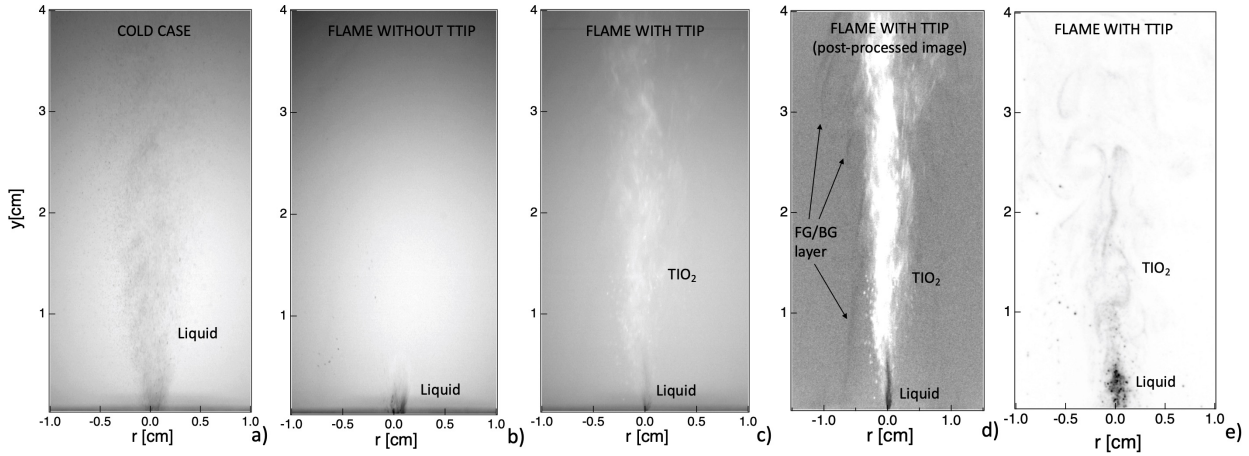


Figure 4: Instantaneous (a-d) shadowgraphy and (e) light scattering images. Liquid phase visualization in (a) the cold and (b) the reactive cases without TTIP injection. (c) Liquid phase and TiO_2 nanoparticles visualization in the reactive case with TTIP injection. (d) Post-processed image for the reactive case to visualize liquid phase, TiO_2 nanoparticles and the flow density variation at the layer between ambient fresh gas and hot burnt gases from the flame. (e) Liquid phase and TiO_2 visualization in the reactive case with TTIP injection using light scattering.

nique, planar information can be obtained. However, a rigorous discrimination between the signal from spray and the signal from TiO_2 nanoparticles is not straightforward. It has been observed that the contribution from the liquid spray scattering is predominant compared to the one from nanoparticles in the region close to the liquid injection. Therefore, it is assumed in the following that in the spray zone close to the burner a high intensity signal corresponds to spray light scattering, whereas low intensity corresponds to TiO_2 nanoparticles. Even if such criterion is arbitrary, the complementary use of shadowgraphy allows to identify the region where the liquid phase is expected to be observed (in our case, for a height above the burner $y < 1$ cm). Indeed in this region, results from light scattering should be analyzed with caution, but outside this region, light scattering information can be used to localize the presence of TiO_2 particles.

4. Characterization of spray flame synthesis

The main processes occurring during the flame synthesis, schematically presented in Fig. 1b, are described here thanks to in situ optical diagnostics, classically used in combustion research.

4.1. Liquid injection and spray

Thanks to shadowgraphy and light scattering measurements, the presence of the spray can be investigated. Instantaneous and time-averaged fields are presented in a blue color palette in Fig. 5 with both techniques. When looking at the instantaneous results, the presence of a central liquid jet core is observed. The liquid is localized in a small region close to the injector nozzle ($y < 0.5$ cm) due to the effect of the dispersion oxygen flow, which leads to the break up of the liquid jet into droplets, together with the effect of the flame high temperature, which results in a rapid evaporation. Occasionally, big droplets can be observed at higher heights above the burner.

It should be noted that some differences are observed between the two techniques. In particular, a dense cylindrical liquid jet seems to be detected by light scattering whereas the atomization seems to occur more rapidly from shadowgraphy results. However, it has to be reminded that the two systems neither present the same sensitivity nor the same resolution of the liquid structures. Moreover, integrated line-of-sight measurements are provided by shadowgraphy, whereas light scattering gives access to planar information. Finally, light scattering results may be affected by the fact that it detects simultaneously both spray and TiO_2 nanoparticles.

In order to verify that spray results from light scattering are reasonable even in presence of TiO_2 nanoparticles, the reactive case without TTIP injection has been considered. The spray region identified by light scattering in this case is indicated by the red isocontour in time-averaged images in Fig. 5. Even if a slightly shorter spray region is identified compared to the flame with TTIP injection, no significant differences are observed so that it can be deduced that the spray region is correctly identified by the light scattering technique even in presence of nanoparticles. Therefore, the differences between results from light scattering and shadowgraphy are most probably due to the intrinsic specificity of these two techniques. Even if a more detailed characterization of the performances of these techniques in the context of flame synthesis is desirable, some common conclusions on the spray process can already be quantified. First, high fluctuations of the spray position are observed (not shown). Second, results are not symmetric, possibly due to the difficulty in obtaining a perfect centering of the liquid injection syringe in the dispersion system. Third, TiO_2 nanoparticles are formed close the spray, indicating that the nanoparticles production is an extremely fast process occurring once the TTIP precursor has evaporated. Finally, it can be said that the spray is not likely to be found for $y > 1$ cm, so that in this zone light scat-

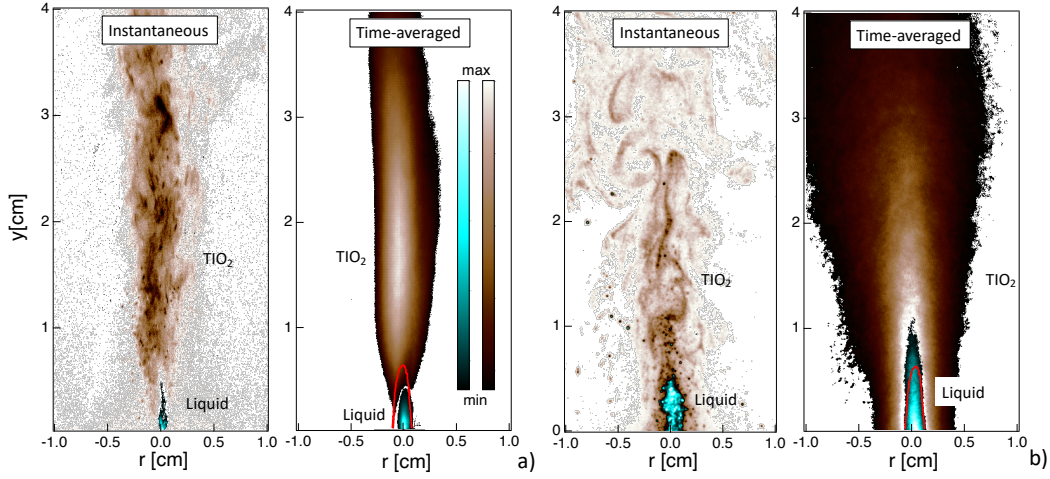


Figure 5: Localization of liquid phase (blue color palette) and TiO_2 nanoparticles (brown palette) via; (a) shadowgraphy and (b) light scattering. Instantaneous (left) and time-averaged (right) results are presented. The red line corresponds to the liquid break-up region for the reactive case without TTIP injection from light scattering measurements.

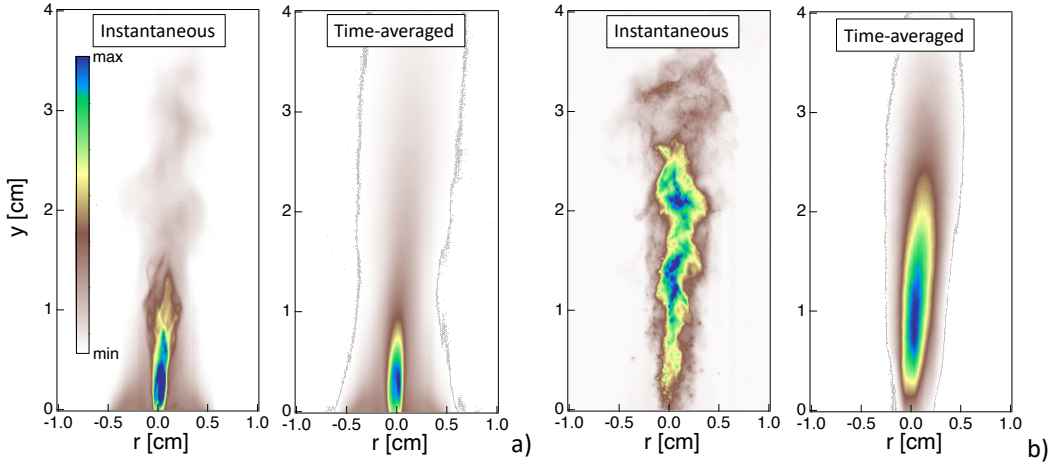


Figure 6: Integrated line-of-sight global emission for the reactive cases (a) without and (b) with TTIP injection. Instantaneous (left) and time-averaged (right) results are presented.

tering from spray can be considered as negligible compared to nanoparticles contribution. Then, results on TiO_2 nanoparticles can be considered with confidence for $y > 1$ cm.

4.2. Flame

The combustion process is investigated here by considering spontaneous emission and OH^* chemiluminescence fields. The global spontaneous emission from the flame contains information on the whole flame emission, while OH^* chemiluminescence can be used to localize the heat release zone. In the presented case, the signal from global spontaneous emission is generally 10 times higher than the one from OH^* .

Spontaneous global emission results for the reactive cases with and without TTIP injection are presented in Fig. 6. Both instantaneous and time-averaged fields are shown. Looking at the instantaneous results, a turbulent flame behaviour can be recognized even if these measurements provide integrated line-of-sight information.

When considering time-averaged results, it can be noticed that the symmetry of the fields is not perfect, similarly to the results for spray in Fig. 4.

Results are quite different between the two cases, indicating that the TTIP addition has a non-negligible effect on spontaneous emission. When looking at the case without TTIP (Fig. 6a), the isopropyl flame and the pilot flames can be discriminated. Indeed, the most relevant emission contribution due to the isopropyl flame is located along the central line at small height above the burner ($y < 0.5$ cm). The pilot flame, localized close to the burner lip, only slightly contributes to the flame emissions. In the case of TTIP addition (Fig. 6b), the maximum values of emission are found far above the burner ($0.5 \text{ cm} < y < 1.5 \text{ cm}$) due to the presence of nanoparticles. In this case, spontaneous emission is the result of both flame and nanoparticles emissions. The maximum values of spontaneous emission for the TTIP injection case is higher of a factor 10, compared to the case

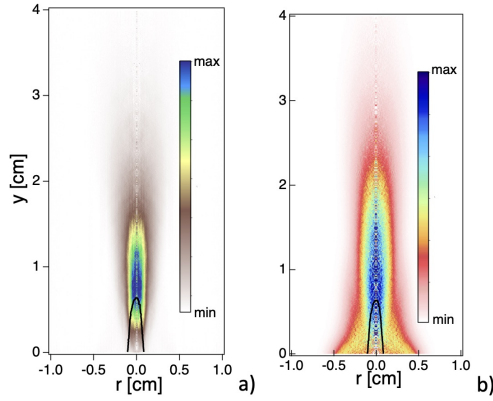


Figure 7: Planar information are extracted using the Abel-inversion (right) on time-averaged results from (a) spontaneous global emission and (b) OH* chemiluminescence results. The black isoline indicates the liquid break-up region.

without TTIP injection. By looking to the instantaneous results in Fig. 6b and by comparing to results from the case without TTIP injection of Fig. 6a, it can be deduced that the contribution from the solid phase is higher than the one from the central flame. The emission from the pilot flame is negligible compared to the global spontaneous emission.

To obtain 2-D planar information, time-averaged results from spontaneous global emission and OH* chemiluminescence for the TTIP injection case have been post-processed using an Abel-inversion transformation considering only the right half-side of the time-averaged results in Fig. 6. Results are illustrated in Fig. 7. The liquid break-up region is indicated by the black line. When looking at the Abel-inverted fields, both spontaneous global emission and OH* chemiluminescence present a similar spatial evolution. In specific, the maxima of flame luminosity and OH* chemiluminescence are located along the centerline. The global emission is 5 times higher than OH* chemiluminescence signal. Once the spray evaporated ($y > 1$ cm), most of the heat is expected to be released in this region ($y < 2$ cm) and post-combustion processes are observed up to $y \approx 4$ cm. Close to the injector, a lower signal intensity is measured compared to the central region, possibly indicating that the pilot flame only slightly contributes to the global heat release even if it is essential for the flame stabilization.

4.3. Particle production

As mentioned above, the presence of TiO₂ nanoparticles can be analyzed by looking at both shadowgraphy and light scattering fields. When looking to results close to the injector (Fig. 5), it can be seen that nanoparticles appear in the close proximity of the spray. This indicates that once the liquid precursor has evaporated, it is rapidly converted into solid phase, confirming that TiO₂ production is governed by fast reactions. Once the particles formed, their localization and concentration seem to be strongly governed by turbulence. In the instantaneous image from shadowgraphy of Fig. 5, it is possible

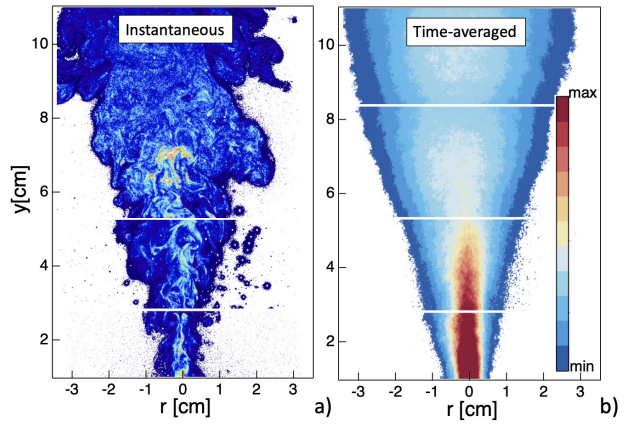


Figure 8: Localization of TiO₂ nanoparticles (brown palette) via light scattering measurements. Random collection of instantaneous images (left) and time-averaged field (right). The images are reconstructed by assembling four series of measurements at four vertical positions of the laser sheet.

to find out the interaction between particles and the turbulent flow. This is even more clear when looking to the instantaneous results of light scattering close the injector (Fig. 5) and along the flame (Fig. 8a). Once TTIP evaporates, TiO₂ nanoparticles are quickly produced in the high heat-release region ($y < 2$ cm). Then, they mainly concentrate along thin ligaments that are stretched and deformed by the turbulent flow eddies and are finally convected downstream the combustion region ($y > 4$ cm).

For higher heights above the burner ($y > 8$ cm), a more homogeneous spatial distribution of the particles is observed due to diffusion effects and a less intense turbulent flow. Time-averaged results of light scattering are presented in Fig. 8b. A very intense signal is observed in the high heat-release region, which rapidly decreases downstream the post-flame region. This high light scattering region seems to coincide with the high flame luminosity zone in Fig. 1a. The light scattering signal depends on particle size and number density. Since the size of the particles is not expected to decrease along the height above the burner, the light scattering field seems to indicate that the nanoparticles are generated close the spray region in large number and that the particles number density subsequently decreases due to collisional processes.

5. Conclusion

The objective of the present work was to improve our understanding of TiO₂ nanoparticles synthesis in turbulent spray flames using in situ optical diagnostics classically used in combustion research. Shadowgraphy, light scattering, global flame luminosity and OH* chemiluminescence measurements were employed in order to study the three main processes that characterize the spray flame. In this way, the liquid break-up, the reactive flow and the TiO₂ particles production were analyzed.

Shadowgraphy measurements showed that it was possible to simultaneously localize the liquid phase, the nanoparticles and the hot/cold layer of the flow. Light scattering results permitted to characterize the TiO₂

nanoparticles distribution in the flame central plane. The liquid is localized in a small region close to the injector nozzle where it is dispersed by the oxygen flow resulting in droplets. The liquid droplets rapidly evaporate due to high temperature of the flame. When TTIP is added to the liquid flow, right after its evaporation and due to its high reactivity, it is immediately converted to TiO₂ nanoparticles. Spontaneous global emission and OH* chemiluminescence results showed quite different reactive flow patterns when considering or not TTIP injection. In the case of TTIP addition maximum emissions are observed far above the burner showing the non-negligible contribution of TiO₂ particles emissions. Finally shadowgraphy and light scattering results at different heights above the burner showed high interactions between nanoparticles and the turbulent eddies. The feasibility of using in situ optical diagnostics from combustion research to obtain information on flame synthesis complementary to the classical ex situ measurements has been proven, even if in future works an optimization of these techniques to flame synthesis is desirable.

Acknowledgments

This work has received funding from the European Research Council (ERC) under the European Union Horizon 2020 research and innovation programme (grant agreement No. 757912).

References

- [1] A. M. M. Sokolowski, A. Sokolowska, B. Gokieli, *J. Aerosol Sci.* 8 (1977) 219.
- [2] S. P. H.K. Kammler, L. Maedler, *Chem. Eng. Technol.* 24 (2001) 583–595.
- [3] W. J. S. L. Madler, S. E. Pratsinis, *J. Mater. Res.* 17 (2002) 1356–1362.
- [4] R. M. S. P. L. Maedler, H.K. Kammler, *Aerosol Sci* 33 (2002) 369–389.
- [5] S. Engel, A. Koegler, Y. Gao, D. Kilian, M. Voigt, T. Seeger, W. Peukert, A. Leipertz, *Appl. Opt.* 51 (2012) 6063–6075.
- [6] R. S. A. Camenzind, S. E. Pratsinis, *Chem. Phys. Lett.* 415 (2005) 193.
- [7] R. Strobel, S. E. Pratsinis, *J. Mater. Chem.* 17 (2007) 4743.
- [8] H. Schulz, L. Madler, S. E. Pratsinis, P. Burtscher, N. Moszner, *Adv. Funct. Mater* 15 (2005) 830.
- [9] F. Schneider, S. Suleiman, J. Menser, E. Borukhovich, I. Wlokas, A. Kempf, H. Wiggers, C. Schulz, *Rev. Sci. Instrum.* 90 (2019) 085108.
- [10] A. J. Grohn, S. E. Pratsinis, K. Wegner, *Chem. Eng. J.* 191 (2012) 491.
- [11] A. J. Grohn, S. E. Pratsinis, A. Sanchez-Ferrer, R. Mezzenga, K. Wegner, *Ind. Eng. Chem. Res.* 10734 (2014) 53.
- [12] S. K. A. K. I. W. C. Weise, J. Menser, *Proc. Combust. Inst.* 25 (2015) 2259–2266.
- [13] A. Rittler, L. Deng, I. Wlokas, A. Kempf, *Proc. Combust. Inst.* 1077 (2017) 36.